Detection of carbon dioxide and hydrogen peroxide on the stratified surface of Charon with JWST

Silvia Protopapa[1*], Ujjwal Raut[2,3], Ian Wong[4,5,6], John Stansberry[6,7,8], Geronimo L. Villanueva[4], Jason Cook[9], Bryan Holler[6], William M. Grundy[7,8], Rosario Brunetto[10], Richard J. Cartwright[11], Bereket Mamo[3,2], Joshua P. Emery[8], Alex H. Parker[12], Aurelie Guilbert-Lepoutre[13], Noemi Pinilla-Alonso[14], Stefanie N. Milam[4], Heidi B. Hammel[15]

[1*]Southwest Research Institute, Boulder, CO, USA.
[2]Southwest Research Institute, San Antonio, TX, USA.
[3]University of Texas at San Antonio, San Antonio, TX, USA.
[4]NASA Goddard Space Flight Center, Greenbelt, MD, USA.
[5]American University, Washington, DC, USA.
[6]Space Telescope Science Institute, Baltimore, MD, USA.
[7]Lowell Observatory, Flagstaff, AZ, USA.
[8]Northern Arizona University, Flagstaff, AZ, USA.
[9]Pinhead Institute, Telluride, CO, USA.
[10]Université Paris-Saclay, CNRS, Institut d'Astrophysique Spatiale, Orsay, France.
[11]Johns Hopkins University Applied Physics Laboratory, Laurel, MD, USA.
[12]SETI Institute, Mountain View, CA, USA.
[13]LGL-TPE, UMR 5276 CNRS, University Lyon 1, ENS, Villeurbanne, France.
[14]Florida Space Institute, University of Central Florida, Orlando, FL, USA.
[15]Association of Universities for Research in Astronomy, Washington, DC, USA.

*Corresponding author(s). E-mail(s): silvia.protopapa@swri.org;

This file includes Supplementary Table 1 and Supplementary Figures 1 to 5.

Supplementary Table 1 Details of the JWST/NIRSpec Observations of Charon (Program ID #1191)

Filename[1]	Date[2]	Time[3]	Obs. #	Grating	Filter	Exp. Time[4]
jw01191004001_03101_00001	2022-09-24	17:35:06.553	004	G140H	F100LP	204.244
jw01191004001_03101_00002	2022-09-24	17:41:49.112	004	G140H	F100LP	204.244
jw01191004001_03103_00001	2022-09-24	17:50:48.902	004	G235H	F170LP	277.189
jw01191004001_03103_00002	2022-09-24	17:58:41.734	004	G235H	F170LP	277.189
jw01191004001_03105_00001	2022-09-24	18:08:48.432	004	G395H	F290LP	554.378
jw01191004001_03105_00002	2022-09-24	18:21:18.447	004	G395H	F290LP	554.378
jw01191005001_03101_00001	2023-04-18	01:29:16.432	005	G140H	F100LP	204.244
jw01191005001_03101_00002	2023-04-18	01:35:51.119	005	G140H	F100LP	204.244
jw01191005001_03103_00001	2023-04-18	01:45:04.734	005	G235H	F170LP	277.189
jw01191005001_03103_00002	2023-04-18	01:53:06.205	005	G235H	F170LP	277.189
jw01191005001_03105_00001	2023-04-18	02:03:04.343	005	G395H	F290LP	554.378
jw01191005001_03105_00002	2023-04-18	02:15:42.999	005	G395H	F290LP	554.378
jw01191103001_03101_00001	2023-04-21	07:00:42.847	103	G140H	F100LP	204.244
jw01191103001_03101_00002	2023-04-21	07:07:23.103	103	G140H	F100LP	204.244
jw01191103001_03103_00001	2023-04-21	07:16:31.149	103	G235H	F170LP	277.189
jw01191103001_03103_00002	2023-04-21	07:24:24.365	103	G235H	F170LP	277.189
jw01191103001_03105_00001	2023-04-21	07:34:30.759	103	G395H	F290LP	554.378
jw01191103001_03105_00002	2023-04-21	07:47:01.158	103	G395H	F290LP	554.378
jw01191106001_03101_00001	2023-04-19	04:59:16.507	106	G140H	F100LP	204.244
jw01191106001_03101_00002	2023-04-19	05:05:51.195	106	G140H	F100LP	204.244
jw01191106001_03103_00001	2023-04-19	05:15:04.809	106	G235H	F170LP	277.189
jw01191106001_03103_00002	2023-04-19	05:23:06.281	106	G235H	F170LP	277.189
jw01191106001_03105_00001	2023-04-19	05:33:04.419	106	G395H	F290LP	554.378
jw01191106001_03105_00002	2023-04-19	05:45:43.074	106	G395H	F290LP	554.378

[1]Data are publicly available from the Space Telescope Science Institute's Mikulski Archive for Space Telescopes: https://mast.stsci.edu/. Details for JWST program #1191 are available at https://www.stsci.edu/jwst/phase2-public/1191.pdf.

[2]Date format: (yyyy-mm-dd); UTC date at the start of exposure.

[3]Time format: (hh:mm:ss.sss); UTC time at the start of exposure.

[4]Exposure Time: (s); Effective exposure time.

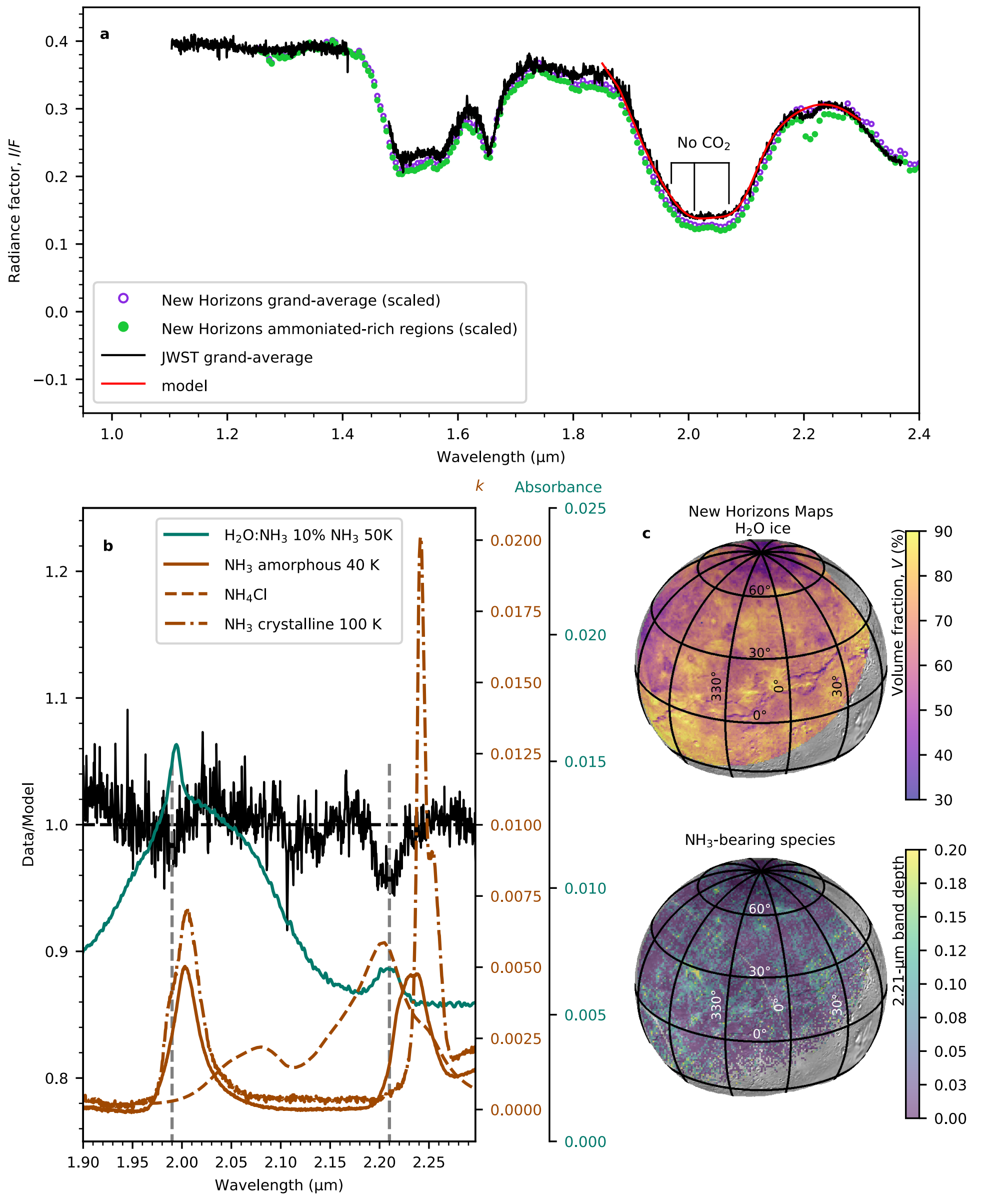

Supplementary Fig. 1 Comparing JWST and New Horizons spectra of Charon with a focus on the 2.21-µm feature. a The JWST/NIRSpec grand-average spectrum of Charon (black line) is plotted alongside the best fit model (red line) for the 2.0-µm region. For comparison, the spectra from the New Horizons/LEISA's C_LEISA_HIRES scan of Charon, normalized to the JWST data at 1.34 µm, are shown [8]. Specifically, the magenta dots illustrate the disk-averaged spectrum of Charon, while the green dots display the spectrum from regions that showcase the most pronounced 2.21-µm absorption band (green to yellow regions in the 2.21-µm band depth map at the bottom of panel c). **b** Displayed here are the residuals (data/model) within the 2.2-µm spectral range. For context, laboratory spectra — both in terms of the imaginary part of the refractive index k (brown lines) and absorbance (teal line) (where a peak in k or absorbance signifies an absorption band) — of amorphous and crystalline NH_3 [80, 81], a H_2O-NH_3 ice mixture containing 10% NH_3 [40], and ammonium chloride (NH_4Cl) [82] are presented. Considering the position and width of the 2.21- and 1.99-µm absorption bands, marked by gray dashed lines, we deduce that NH_3 diluted in H_2O is the best candidate for the nature of the NH_3-bearing species on Charon. **c** The top and bottom panels, respectively, show the volume fraction of crystalline H_2O ice and the 2.21-µm band depth map of Charon. Both are derived from a pixel-by-pixel Hapke radiative transfer model analysis of the New Horizons C_LEISA_HIRES scan [8]. Source data are provided as a Source Data file.

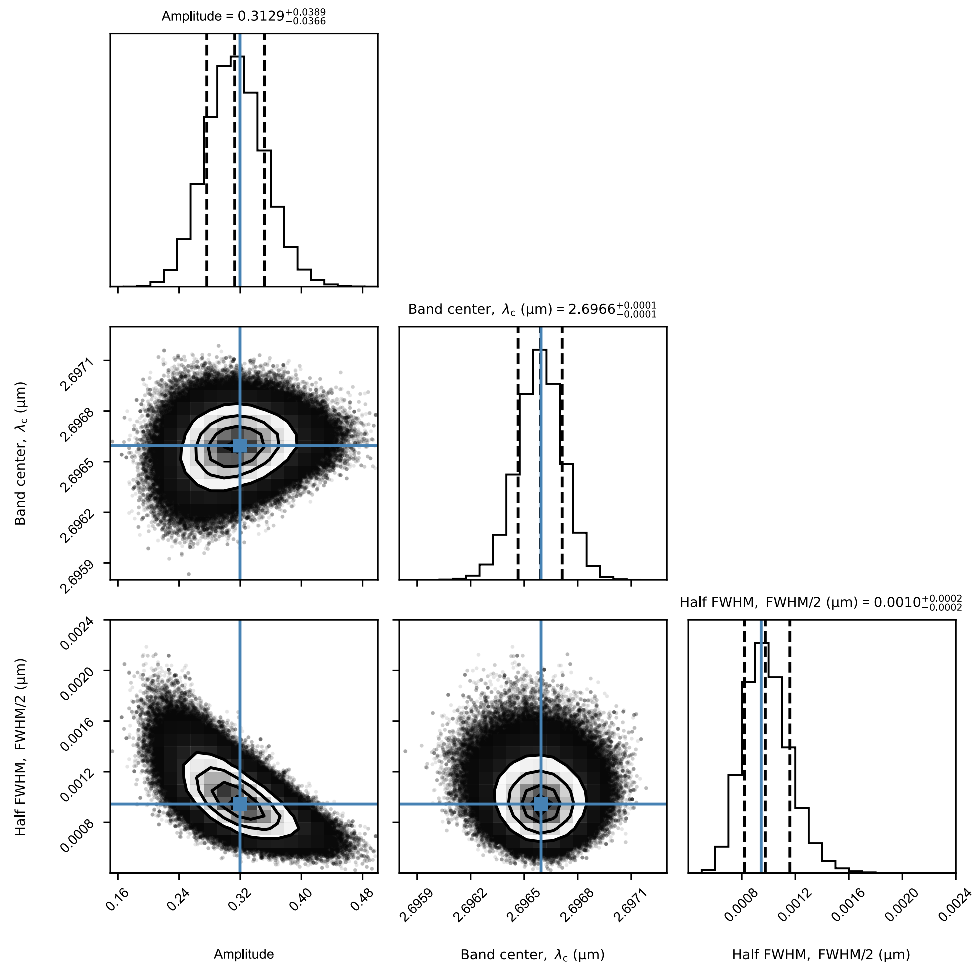

Supplementary Fig. 2 Markov Chain Monte Carlo (MCMC) parameter exploration of the Lorentzian fit to the 2.7-µm $\nu_1 + \nu_3$ **CO_2 band.** This corner plot visualizes the 1D and 2D posterior distributions resulting from the MCMC fitting of the 2.7-µm CO_2 absorption band using a Lorentzian model. The explored parameters include amplitude, band center λ_c, and half of the full width at half maximum (FWHM). The contours represent the 1-σ, 2-σ, and 3-σ confidence intervals, derived from the quantile levels of 16%, 50%, and 84%. The MCMC simulation, conducted using the `emcee` Python library, used 1000 walkers and a chain length of 3000 steps. When generating the posterior distributions, the first 10% of the chains was discarded. The blue markers represent the best-fit parameters derived using a Levenberg-Marquardt minimization process prior to the MCMC run. These parameters are shown in the spectral fit in Figure 2c.

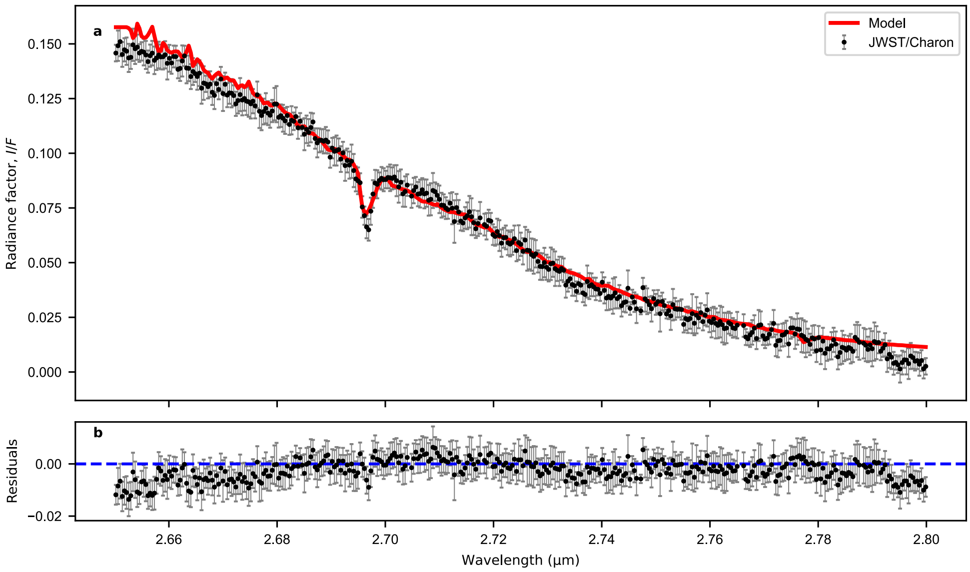

Supplementary Fig. 3 CO_2 abundance as derived from the 2.7-μm $\nu_1 + \nu_3$ absorption band. **a** The grand-average spectrum of Charon, obtained by JWST/NIRSpec (represented by black points) along with the corresponding 1-σ errors (gray bars), is plotted against the best-fit model (red line) for the 2.7-μm region. **b** The residuals between the data and the best fit are shown. The model consists of an areal mixture of 80% crystalline H_2O ice, 18% amorphous H_2O ice, and 2% crystalline CO_2. Source data are provided as a Source Data file.

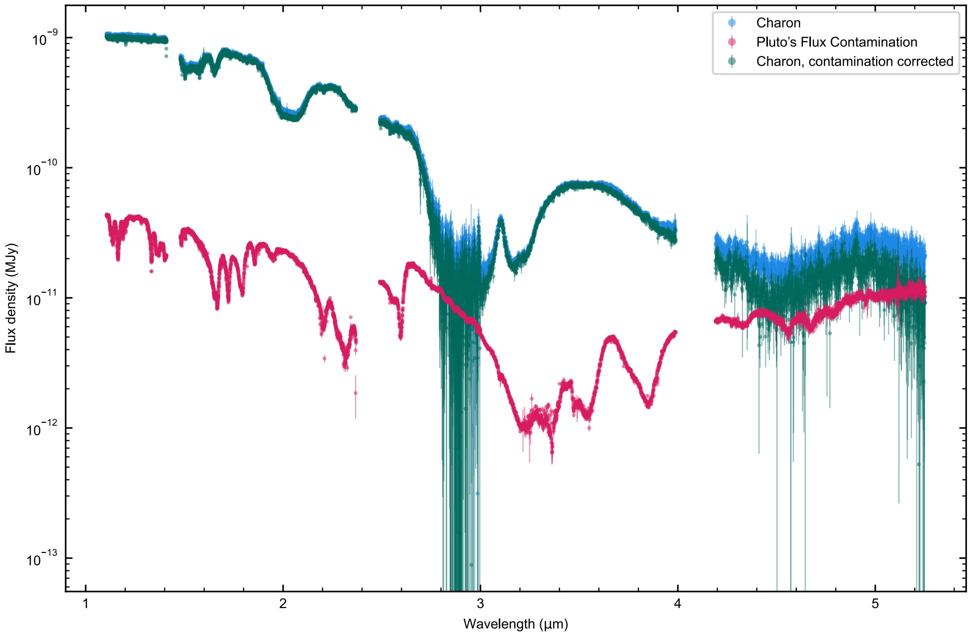

Supplementary Fig. 4 Charon's spectrum before and after correcting for Pluto's flux contamination. The JWST spectrum of Charon corresponding to Observation #103 before (blue) and after (green) correction for Pluto's flux contamination (red) is shown, with 1-σ errors indicated for each spectrum. The comparison highlights that Pluto and Charon do not share the same spectral features. On average, Pluto's flux contamination contributes 5% across the spectral range. However, in the specific wavelength ranges between 2.8 and 3 µm, and between 4.19 and 5.3 µm, the contamination increases significantly to 47% and 38%, respectively. Source data are provided as a Source Data file.

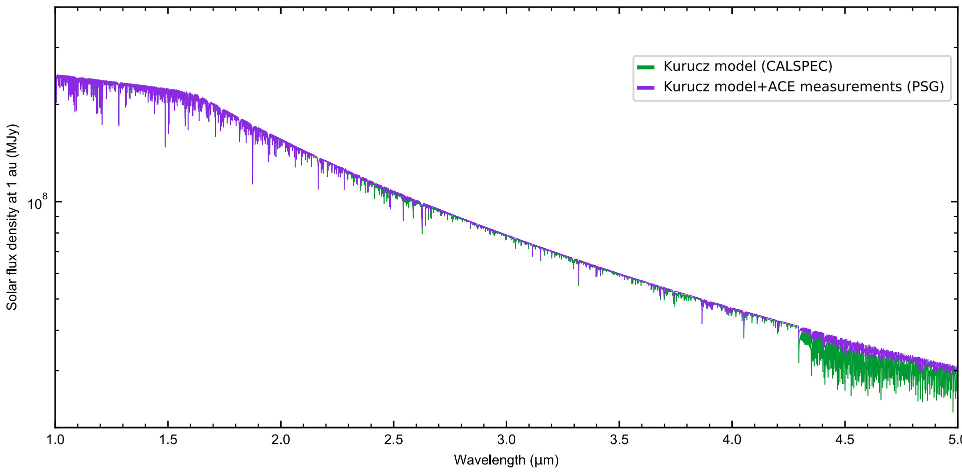

Supplementary Fig. 5 Comparison of measured and synthetic solar spectra. The solar spectrum at 1 au, as modeled by Kurucz (represented by the green line and sourced from the CALSPEC database), is compared with the solar spectrum implemented by the Planetary Spectrum Generator (PSG). The latter combines the Kurucz model at short wavelengths up to 2.0 µm with measurements from the ACE instrument onboard SCISAT-1 beyond 2 µm. Both spectra are shown at a resolving power of 5000. As expected, there is perfect agreement between the two spectra at shorter wavelengths. However, the CALSPEC model clearly does not reproduce the observed spectrum beyond 4.3 µm. Source data are provided as a Source Data file.